Chapter 5.

Adsorption and Reaction of Methanol and Acetic Acid on TiO_2(001) Studied by Scanning Tunneling Microscopy and Temperature Programmed Desorption

Abstract

Chemical activity of two kinds of Ti cation sites exposed on $TiO_2(001)$ surface was evidently clarified by investigating the adsorption sites and reactivity of methanol and acetic acid in atomic scale by means of scanning tunneling microscopy (STM) and temperature programmed desorption (TPD). Recently I have reported the "bleachers-like structure" of $TiO_2(001)$, on which homogeneously arranged two kinds of Ti cations are observed by STM. They were assigned fourfold and fivefold coordinated Ti cations. Adsorption and reaction of methanol showed that fourfold coordinated Ti had higher activity such as dissociative adsorption of methanol and decomposition of methoxy, whereas fivefold coordinated Ti had rather mild activity. In TPD for acetic acid on the bleachers-like structure, decomposition at 430 K and desorption of ketene at 620 K was detected and the active site for the reactions were assigned to fourfold and fivefold coordinated Ti, respectively, comparing with $TiO_2(110)$. On reduced $TiO_2(001)$, low temperature re-annealing at 390-660 K caused drastic change in surface structure and reactivity

5.1 Introduction

Metal oxides are key materials for many industrial technologies such as catalysts, gas sensors, semiconductor devices, etc. It plays an important role for design and control catalytic function to clarify the surface structure, active site and reaction intermediate on metal oxide surfaces in atomic scale. Among a variety of oxides, the (110) surface of rutile-type TiO_2 has been most extensively studied as a representative oxide surface.[1,2] A TiO_2(110) surface is the most stable among the low-index planes of rutile-type TiO_2. The surface structure of TiO_2(110) is almost identical to bulk termination as proved by experimental techniques[3,4] and theoretical calculations.[5,6] One-dimensional rows of fivefold coordinated Ti atoms and bridged O atoms along the [001] direction are arranged alternately, which are clearly observed by scanning tunneling microscopy (STM) and noncontact atomic force microscopy (NC-AFM), respectively. Formic acid dissociatively adsorbed as formate anion TiO_2(110) bridging two fivefold coordinated Ti cations.[7-9] Adsorbed formate mainly decomposed to carbon monoxide and hydrogen via unimolecular dehydrogenation, while reaction path switched to bimolecular dehydration with gas phase formic acid under formic acid ambient.[10] The TiO_2(110)-(1×1) surface was stable during the catalytic reaction of formic acid[10,11] and the surface reaction of acetic acid,[12] where each carboxylate intermediate on (1×1) surface was resolved by STM. However, recent STM investigations revealed that surface structure of TiO_2(110) drastically changed by annealing the surface in the presence of oxygen atmosphere due to the reaction of oxygen with Ti^{n+} cations diffused to the surface from interstitial site of bulk TiO_2, forming the added layer of TiO_x (x =1-2) depending on the conditions.[13-15]

In contrast, there has been rather limited number of studies reported on TiO_2(001). All the exposed Ti on TiO_2(001) atoms take fourfold coordination, doubly unsaturated

compared with Ti atoms in the bulk. This surface is non-polar, but unstable due to low ligand coordination. Theoretical calculations revealed that the (001) termination had significantly high surface energy comparing with the (110) and the (100) termination, and surface reconstruction was suggested to stabilize the surface.[5,6] In fact, two ordered phases have been observed by low energy electron diffraction (LEED) on TiO_2(001) depending on annealing temperature.[16,17] {011}-faceted and {114}-faceted structural models identical to each bulk-terminated structure were proposed for the lower- and higher- temperature phase, respectively, based on kinematic LEED analysis.[17] To date, some structural analyses of TiO_2(001) surfaces by scanning probe microscopies (SPM) have been reported. In the first STM observation of TiO_2(001), faceted structures which included mainly (011) planes were observed after annealing to 783 K for 30 min-2 h.[18] Following STM and AFM studies on TiO_2(001) also showed faceted or disordered reconstruction after thermal treatments under UHV.[19-21] Recently, Nörenberg et al. reported another phase of TiO_2(001), which appeared under non-equilibrium conditions.[22] Network-like structure with $(7\sqrt{2}\times\sqrt{2})$ periodicity was observed after annealing the sample to the higher temperatures than 1473 K with heating and cooling rate of 100 K s^{-1}.

Barteau and co-workers [23-27] studied surface reactions on TiO_2(001) by temperature-programmed desorption (TPD) for the two ordered phases reported by the LEED study.[16,17] Chemical activity of the surfaces was extremely different among an Ar^+-sputtered surface, a lower-temperature phase, and a higher-temperature phase. Especially on the higher-temperature phase, which was assigned to {114}-faceted surface,[17] products of dimerization reaction were detected, such as dimethyl ether and acetone from methanol and acetic acid, respectively. These products were not detected on the lower-temperature phase as well as on the most stable TiO_2(110) surface. The active sites

of the dimerization reactions were proposed to be fourfold coordinated Ti atoms remaining on the faceted surface. However, investigation on atomic-scale structures and active site of ordered $TiO_2(001)$ surfaces has not been so successful, partially because it is difficult to prepare a homogeneous structure on $TiO_2(001)$, which is tolerable for precise measurements with high spatial resolution by SPM.

In chapter 3 and 4 I have succeeded in visualizing the higher-temperature phase of $TiO_2(001)$ surface in atomic scale by STM for the first time. The surface was not a facet but a rather flat structure consisted of row structures along the [110] and [1$\bar{1}$0] with narrow terraces and steps on its slope, which I named "bleachers-like structure". I proposed a new structural model including fourfold and fivefold coordinated Ti atoms, based on atom-resolved STM images. In this chapter I report about the adsorption and reaction of methanol and acetic acid on the bleachers-like structure on $TiO_2(001)$. The difference of reactivity of two kinds of coordinatively unsaturated Ti atoms was clearly revealed by STM and TPD.

5.2 Experimental

The experiments were performed in two different UHV chambers. STM images were obtained in an ultrahigh vacuum (UHV) STM (JEOL JSTM 4500VT) equipped with an Ar^+ ion gun and a LEED optics. The base pressure was $1x10^{-8}$ Pa. A polished $TiO_2(001)$ wafer of $6.5 \times 1 \times 0.25$ mm^3 (Earth Chemical) was used after deposition of Ni film on the rear side of the sample to resistively heat the sample on a sample holder. Heating rate and cooling rate was controlled to be 7-10 K s^{-1}. The $TiO_2(001)$ surface was cleaned with cycles of Ar^+ ion sputtering (3 keV for 2 min) and annealing under UHV at ca. 900 K.

All STM images displayed in this report are constant current topographies (CCT) obtained at room temperature (RT) with electro-chemically etched W tips. The surface temperature of the crystal was monitored by an infrared radiation thermometer.

TPD spectra were measured in an UHV chamber equipped with Ar^+ ion gun, a LEED optics and quadrapole mass spectrometer. The base pressure was $1x10^{-8}$ Pa. A polished $TiO_2(001)$ wafer of $16\times 8\times 1$ mm^3 (Earth Chemical) with deposited Ni film on the rare side was fixed by Ta sample holder with another $TiO_2(001)$ wafer without Ni film, sandwiching a small Ta foil with a spot-welded chromel-alumel thermocouple. Exposed area of the sample available for TPD was 8×8 mm^2. TPD of $TiO_2(001)$ was performed in the same way.

Methanol (Wako, contamination less than detection limit) and acetic acid (Wako, 95 % purity) used in this study was purified by repeated freeze-pump-thaw cycles and introduced into the chamber by back-filling.

5.3 Results

Figure 5.1a shows a large-scale ($140\times$ 140 nm^2) STM image of $TiO_2(001)$ surface after Ar^+-sputtering followed by annealing to 1050 K under UHV. It was not a previously reported facet structure, but a rather flat latticework structure consisted of row structures running along the [110] and [$1\bar{1}0$] directions. I have confirmed by STM that the identical structure shown in figure 5.1a covered almost the whole surface and was reproduced after every Ar^+-sputtering and annealing cycle. Figure 5.1b shows a STM image of a smaller area (18.0×18.0 nm^2). The row structures have narrow terraces (for example A, B and C) and steps on their slope, accordingly I named the structure "bleachers-like structure". The

height of each step was 0.30 nm and the average slope was corresponding to the (114) plane. Figure 5.1c shows a magnified image of the topmost terrace of a bleachers-like row. Units of three bright spots were arranged with a regular interval of 0.65 nm along the row axis. In STM images obtained in positive sample bias conditions, distribution of empty states nearby the Fermi energy on the surface is visualized. As mentioned in the introduction session, fivefold coordinated Ti atoms were visualized as bright spots by STM on TiO_2(110) surface. Therefore, the bright spots in figure 5.1c are assigned to exposed Ti cations, as I followed to the case of TiO_2(110). Detailed discussions were already described in chapter 4. Among the three bright spots, the middle one (filled circle) was brighter than other two (empty circle).

Figure 5.2 shows the structural model of the bleachers-like structure based on atom-resolved STM images. The structure consists of suboxide rows placed on the bulk-terminated TiO_2(114) surface. Stoichiometry of the added suboxide rows were Ti_7O_{12} ($TiO_{1.71}$) at the topmost terrace, and T_7O_{11} ($TiO_{1.57}$) at other narrow terraces on the slope. The middle and side bright spots shown in Figure 5.1c were assigned to fourfold and fivefold coordinated Ti atoms, respectively. Assignment of the bright spots was supported by formic acid and methanol adsorption experiments (chapter 4). The structural model in Figure 5.2 is also suitable to a crossing point of two perpendicular rows (chapter 4) and pyramidal structure (chapter 6). Hereinafter "TiO_2(001)" without any mention denotes the bleachers-like structure prepared by identical condition to that shown in figure 5.1.

Figure 5.3a and 5.3b shows STM images of TiO_2(001) after exposure to methanol at RT. Adsorbates with 0.18 nm height were observed as bright spots on the row structures and increased with exposure. They were assigned to dissociatively adsorbed methoxy by the following scheme:

$$CH_3OH(g) + O(s) \rightarrow CH_3O(a) + OH(a) \qquad (1)$$

At low exposure, methanol preferentially adsorbed on the middle bright spots,(Figure 5.3a) which was assigned to fourfold coordinated Ti in figure 5.2. I regarded the partiality of methanol adsorption site as a support for the assignment of the middle bright spot to fourfold coordinated Ti because no methoxy was observed on TiO_2(110) surface, on which only fivefold coordinated Ti atoms are exposed (chapter 4). On TiO_2(110) no features assignable to adsorbates were observed by STM even after exposure to 33 L of methanol at RT (data not shown here). After excess exposure to methanol, methoxy on fivefold coordinate Ti also appeared (Figure 5.3b). Only one methoxy adsorbed on one Ti atom, for both of fourfold and fivefold coordinated Ti. Adsorption of methoxy made no additional subspots in LEED.

Relation between methoxy coverage and methanol exposure was shown in Figure 5.4a, which was obtained by repeated methanol exposure and STM observation cycles at the same area shown in figure 5.3a and 5.3b. Horizontal axis of the graphs in figure 5.4 means the total exposure to methanol during repeated exposure and STM imaging cycles. Methoxy coverage was determined by counting the number of methoxy in STM images. Coverage of methoxy on fourfold coordinated Ti approached to saturation after 3.0 L of exposure, while that of methoxy on fivefold coordinated Ti rapidly increased at exposure between 3.0 L to 18 L. In figure 5.4b the sticking coefficient on fourfold and fivefold Ti atoms during each exposure was plotted against total exposure. It is quite reasonable that sticking coefficient onto fourfold coordinate Ti decreases with increase of exposure because number of empty sites decreased. On the other hand, sticking coefficient onto fivefold coordinated Ti showed strange behavior: sticking coefficient increased until 18 L in spite of slight increase of coverage. I concluded that methoxy on fivefold coordinated Ti was migrated from neighboring fourfold coordinated Ti due to repulsive interaction. Fourfold coordinated Ti is active for dissociative adsorption of methanol, on the other hand fivefold

coordinated Ti is not so active to dissociate O-H bond of methanol, but able to be an adsorption site of methoxy once produced on fourfold coordinated Ti.

Figure 5.5 shows TPD spectra measured for $TiO_2(001)$ surface exposed to various amount of methanol at 240 K. Molecularly adsorbed methanol desorbed around 300 K, which corresponding to previous TPD results from $TiO_2(001)$[25] and $TiO_2(110)$.[28] At low exposure, only reaction product from methoxy was methane, which desorbed at 525 K (figure 5.5a). At higher exposure, additional methanol desorption at 480 K appeared (figure 5.5b) and increased with exposure (figure 5.5c). It was assigned to recombination desorption of methoxy and hydroxyl via inverse reaction of eq. (1). Small amount of broad CO desorption was detected around 300-500 K. It was confirmed being due to residual CO adsorption to the sample holder by blank TPD measurement without methanol exposure. Other carbon-contained products such as formaldehyde, dimethylether and carbon dioxide were not detected.

The peak temperature of CH_4 did not depend on the coverage of methoxy. The results indicated that CH_4 desorption was first-order reaction and rate determining step was C-O bond breaking written in eq. (2):

$$CH_3O(a) \rightarrow CH_3(a) + O(a) \qquad (2)$$

$$CH_3(a) + H(a) \rightarrow CH_4(g) \qquad (3)$$

Activation energy E_a of a first-order reaction can be derived from $\ln(T_p^2/\beta) = E_a/(RT_p) + \ln[E_a/(R\nu)]$,[29] where T_p, β, R and ν represent peak temperature, heating rate, gas constant and pre-exponential factor. The value of 146 kJ mol^{-1} is obtained for CH_4 desorption at 525 K assuming a pre-exponential factor of 10^{13} s^{-1}. Further decomposition of methyl species was thought not to occur because neither H_2 nor CO desorption peak through eq. (4)-(6) appeared, but the possibility was not excluded that H_2 and CO desorbed above 600 K and the peaks were hidden by rapid increase of background pressure.

$CH_3(a) \rightarrow C(a) + 3H(a)$ (4)

$2H(a) \rightarrow H_2(g)$ (5)

$C(a) + O(a) \rightarrow CO(g)$ (6)

Figure 5.6 shows the same area of $TiO_2(001)$ before and after exposure to 3.0 L of CH_3COOH at RT. Adsorbates observed as bright spots in Figure 5.6b were assigned to acetate anions, which adsorbed dissociatively adsorbed to Ti cation sites by the following scheme:

$CH_3COOH(g) + O(s) \rightarrow CH_3COO(a) + OH(a)$ (7)

As shown in the magnified image of figure 5.6b, acetate anions adsorbed to fourfold and fivefold coordinated Ti almost at random. The result is comparable with formic acid adsorption on $TiO_2(001)$ described in chapter 4. Height of acetate was 0.23 nm, which is a reasonable value comparing with the value of a formate on the bleachers-like structure, 0.17 nm. Only one acetate adsorbed on one Ti atom, for both of fourfold and fivefold coordinated Ti, similar to methoxy adsorption. Adsorption state of acetate is not determined only from STM images. I tentatively assign acetate on fourfold and fivefold coordinated Ti to bidentate and unidentate, respectively. Adsorption of acetate right upon a Ti atom, not between two Ti atoms observed in the STM image excluded the possibility of bridge configuration. The distance of 0.65 nm between two fourfold or fivefold coordinated Ti atoms is too far for an acetate to adsorb with bridge configuration.

Figure 5.7a shows TPD spectra measured for $TiO_2(001)$ bleachers-like structure after exposure to 6.0 L of CH_3COOH at 295 K. Decomposition products such as CH_4, H_2, CO_2 and CO was desorbed at 430 K, 530 K, 530 K and 560 K, respectively (eq. (8)-(10)), and dehydration product, ketene (CH_2CO), was desorbed at 630 K (eq. (11)). CO desorption at 690 K is due to burning of completely decomposed atomic carbon (eq. (6)).

$CH_3COO(a) + O(s) \rightarrow CH_3(a) + CO_3(a)$ (8)

$$CH_3(a) + H(a) \rightarrow CH_4(a) \quad (9)$$

$$CO_3(a) \rightarrow CO, CO_2 + O(s) \quad (10)$$

$$CH_3COO(a) \rightarrow CH_2CO\,(g) + OH(a) \quad (11)$$

Figure 5.7b shows TPD spectra measured for TiO_2(110)-(1x1) after exposure to 4.0 L of CH_3COOH at 295 K. TPD result for CH_3COOH on TiO_2(110) was not found in preceding literatures in my knowledge. Ketene desorbed at 580 K as the main product, and small amount of CH_4, CO and H_2 was also detected as byproducts. Maybe CO desorbed above 700 K through atomic carbon burning, but was not quantified due to rapid increase of background CO pressure.

Relative yields of desorption species of the TPD shown in figure 5.7 were displayed in table 5.1. The activation energies of ketene desorption on TiO_2(001) and (110) were 160 kJ mol^{-1} and 148 kJ mol^{-1} calculated by the equation above assuming first-order reaction and pre-exponential factor of 10^{13} s^{-1}. The values are in good agreement with a previous TPD study. Ketene desorption at 610 K was reported on the lower-temperature phase of TiO_2(001) with the heating rate of 1.2 K s^{-1} and the activation energy of 170 kJ mol^{-1} was obtained in the same way.

5.4 Discussion

Explanation and discussion of the atom-resolved STM images and the structural models were described in detail in chapter 4, so that I will herein lay emphasis on reactivity of TiO_2(001) predicating on the structural model shown in figure 5.2.

5.4.1 Distinction of Reactivity between Two Kinds of Ti Atoms: Adsorption and Reaction of Methanol

Preferential adsorption of methoxy in figure 5.3 indicates the difference of chemical property between two kinds of exposed Ti shown in figure 5.1c, which were assigned to fourfold and fivefold coordinated Ti atoms (figure 5.2). In the dissociative adsorption process of eq. (1), not only Ti but also surface oxygen were involved. Therefore local geometry and electronic states of a neighboring atom are also important for the process. Nevertheless I regarded the coordination of Ti as the essential factor because there is always neighboring oxygen atoms with similar unsaturated coordination and similar distance for both kinds of Ti atoms.

TPD spectra in figure 5.4 evidently revealed that chemical reactivity of these two Ti is completely distinct in thermal reactions. Desorbed products from methoxy were CH_4 and CH_3OH, which were desorbed at 530 K and 490 K, respectively. At low methoxy exposure, only CH_4 at 530 K was detected while amount of desorbed CH4 was saturated and CH_3OH desorption at 490 K was increased at high methoxy coverage. The STM images in figure 5.3 showed that methoxy preferentially adsorbed to fourfold coordinated Ti at low methanol exposure and thereby that CH_4 was produced from methoxy on fourfold coordinated Ti, and methoxy on fivefold coordinated Ti (and maybe a part of that on fourfold coordinated Ti) recombinated and desorbed as methanol through inverse reaction of eq. (1). The results clearly distinct reactivity of two kinds of Ti atoms: fourfold coordinated Ti has high reactivity (C-O bond breaking) and fivefold coordinated Ti has mild reactivity (recombination of methoxy and hydroxyl).

5.4.2 Reaction of Acetate

On $TiO_2(110)$, carboxylic acids adsorb on bridge sites and each carboxylate species has been visualized by STM.[7,8,12] In-situ observation of reaction of acetate on $TiO_2(110)$ was reported by Onishi et al.[12] Number of acetate decreased in first-order with a rate constant of $(4\pm 1)\times 10^{-3}$ s^{-1} during thermal reaction from 510 K to 540 K. It was in good agreement with the value of 3.3×10^{-3} s^{-1} at 540 K, which was acquired from the activation energy of 160 kJ mol^{-1} for the ketene desorption in this study, assuming first-order kinetics and a pre-exponential factor of 10^{13} s^{-1}. Onishi et al. also reported that immobile byproducts with larger height than acetate were observed and proposed possibility of carbonates. It was in accord with desorption of CH_4 and CO_2 as byproducts through eq. (8)-(11).

It is difficult to directly determine the adsorption site and reactivity of acetic acid directly from STM images in figure 5.6 as the case of methanol, because acetate adsorbed almost equivalently on fourfold and fivefold coordinated Ti. However, it would be possible to assign the activity of each Ti sites to acetate thermal reaction with $TiO_2(110)$. TPD spectra in figure 5.6a indicate existence of two kinds of activation site on $TiO_2(001)$: one is active to ketene formation at 630 K and the other to decompose acetate at 430 K. The former is proposed to fivefold coordinated Ti because ketene desorption and byreaction to form CH_4 implies the similarity to fivefold coordinated Ti atoms on $TiO_2(110)$. The latter with higher activation is possibly fourfold coordinated Ti. Reactivity of fivefold coordinated Ti on $TiO_2(001)$ and $TiO_2(110)$ is similar but not the same. On $TiO_2(001)$, ratio of selectivity of decomposition to produce CH_4 is larger and complete decomposition to C(a) and O(a) occurred, too. That is due to difference in structure and electronic state between the two surfaces, but adsorption state of acetate, bridge on $TiO_2(110)$ and

unidentate on TiO_2(001), may be also one of factors.

5.4.3 Comparison with Previous Studies

Kim and Barteau have reported the TPD results of methanol and acetic acid on TiO_2(001) surface.[24,25] Different reactivities emerged depending on surface structures. Unimolecular reactions, formaldehyde from methoxy and ketene from acetate, were main path on the lower-temperature phase and additional bimolecular reaction path opened on the higher-temperature phase, dimethylether from methoxy and acetone from acetate. They assigned the activation site for unimolecular reaction to fivefold coordinated Ti and that for bimolecular reaction to fourfold coordinated Ti, based on bulk-terminated (011) and (114) faceted structural models presented in ref [17] for the lower- and higher- temperature phase, respectively.

In the present work, only one methoxy (or acetate) adsorbed on an exposed Ti was observed by STM (figure 5.3 (figure 5.6)) and no bimolecular product such as dimethylether (acetone) was detected in TPD (figure 5.5 (figure 5.7)). It is probably due to the difference of the atomic scale structure between that in ref. 24, 25 and this study, though LEED pattern indicate the same long-range periodicity. In the previous STM and AFM works on TiO_2(001), surface morphology and roughness were varied work by work while the same LEED pattern as ref. [17] was referred to be observed. In my experiments, various phases appeared such as hill-like structure and particle-like structure depending on sample treatment.[30] The LEED pattern of higher temperature phase in the previous studies might be caused by other (114)-(1x1) reconstructed structures, or by minor but large domains enough to provide diffraction patterns domains of the bleachers-like structure. In ref. [24,25], the sample was cleaned by Ar^+-sputtering and annealing for longer time than my work, and

the different surface structure with (114)-(1x1) periodicity would be constructed.

Cautious care is necessary to construct a homogeneous structure on TiO_2(001), especially for investigation of reaction site in an atomic scale because the surface pretreatment extensively affects reactivity of the surface. The result of methanol TPD from TiO_2(001) after Ar^+-sputtering and annealing to 900 K reported in ref. [31] was completely different from both of ref. [25] and this work: main desorbed products were H_2, CO and CH_3OH. In addition, particle-covered surface on reduced TiO_2(001) after reannealing showed completely different reactivity from bleachers-like structure (figure 5.8) as described in former session, although diffraction pattern higher-temperature phase remained.

5.5 Summary

Adsorption and reaction of methanol and acetic acid on the homogeneous "bleachers-like rows" on TiO_2(001) were investigated by STM and TPD. Methanol adsorption and reaction evidently revealed the difference of reactivity between two kinds of exposed Ti atom, which were assigned to fourfold and fivefold coordinated Ti atoms. Fourfold coordinated Ti had higher activity, such as dissociative adsorption of methanol to methoxy at RT and C-O bond breaking of methoxy to form CH_4 at 520 K, while fivefold coordinated Ti showed mild activity. The difference in reactivity was also reflected to thermal reaction of acetic acid. The active sites for decomposition at 430 K and ketene desorption at 620 K of acetate was proposed to fourfold coordinated and fivefold coordinated Ti, respectively, comparing with TiO_2(110).

Reference

(1) Lai, X.; Clair, T. P. S.; Valden, M.; Goodman, D. W. *Prog. Surf. Sci.* **1998**, *59*, 25-52.

(2) Diebold, U. The Structure of TiO2 Surfaces. In *Chemistry and Physics of Solid Surfaces*; King, D. A., Woodruff, D. P., Eds.; Elsevier: Amsterdam, 2001; Vol. 9; pp 443-484.

(3) Maschhoff, B. L.; Pan, J. M.; Madey, T. E. *Surf. Sci.* **1991**, *259*, 190.

(4) Charlton, G.; Howes, P. B.; Nicklin, C. L.; Steadman, P.; Taylor, J. S. G.; Muryn, C. A.; Harte, S. P.; Mercer, J.; McGrath, R.; Norman, D.; Turner, T. S.; Thornton, G. *Phys. Rev. Lett.* **1997**, *78*, 495-498.

(5) Ramamoorthy, M.; Vanderbilt, D.; King-Smith, R. D. *Phys. Rev. B* **1994**, *49*, 16721-16727.

(6) Muscat, J.; Harrison, N. M. *Surf. Sci.* **2000**, *446*, 119-127.

(7) Onishi, H.; Iwasawa, Y. *Chem. Phys. Lett.* **1994**, *226*, 111-114.

(8) Onishi, H.; Fukui, K.; Iwasawa, Y. *Bull. Chem. Soc. Jpn.* **1995**, *68*, 2447-2458.

(9) Chambers, S. A.; Thevuthasan, S.; Kim, Y. J.; Herman, G. S.; Wang, Z.; Tober, E.; Ynzunza, R.; Morais, J.; Peden, C. H. F.; Ferris, K.; Fadley, C. S. *Chem. Phys. Lett.* **1997**, *267*, 51-57.

(10) Onishi, H.; Aruga, T.; Iwasawa, Y. *J. Catal.* **1994**, *146*, 557-567.

(11) Iwasawa, Y.; Onishi, H.; Fukui, K. *Topics in Catal.* **2001**, *14*, 163-172.

(12) Onishi, H.; Yamaguchi, Y.; Fukui, K.; Iwasawa, Y. *J. Phys. Chem.* **1996**, *100*, 9582-9584.

(13) Onishi, H.; Iwasawa, Y. *Phys. Rev. Lett.* **1996**, *76*, 791.

(14) Li, M.; Hebenstreit, W.; Gross, L.; Diebold, U.; Henderson, M. A.; Jennison, D. R.; Schultz, P. A.; Sears, M. P. *Surf. Sci.* **1999**, *437*, 173-190.

(15) Bennett, R. A.; Stone, P.; Price, N. J.; Bowker, M. *Phys. Rev. Lett.* **1999**, *82*, 3831-3834.

(16) Tait, R. H.; Kasowski, R. V. *Phys. Rev. B* **1979**, *20*, 5178-5191.

(17) Firment, L. E. *Surf. Sci.* **1982**, *116*, 205-216.

(18) Poirier, G. E.; Hance, B. K.; White, J. M. *J. Vac. Sci. Technol. B* **1992**, *10*, 6-15.

(19) Nörenberg, H.; Dinelli, F.; Briggs, G. A. D. *Surf. Sci.* **2000**, *446*, L83-L88.

(20) Antonik, M. D.; Edwards, J. C.; Lad, R. J. *Mat. Res. Soc. Symp. Proc.* **1992**, *237*, 459-464.

(21) Watson, B. A.; Barteau, M. A. *Chem. Mater.* **1994**, *6*, 771-779.

(22) Nörenberg, H.; Dinelli, F.; Briggs, G. A. D. *Surf. Sci.* **1999**, *436*, L635-L640.

(23) Kim, K. S.; Barteau, M. A. *Langmuir* **1990**, *6*, 1485-1488.

(24) Kim, K. S.; Barteau, M. A. *J. Catal.* **1990**, *125*, 353-375.

(25) Kim, K. S.; Barteau, M. A. *Surf. Sci.* **1989**, *223*, 13-32.

(26) Idriss, H.; Kim, K. S.; Barteau, M. A. *Surf. Sci.* **1992**, *262*, 113-127.

(27) Barteau, M. A. *Chem. Rev.* **1996**, *96*, 1413-1430.

(28) Henderson, M. A.; Otero-Tapia, S.; Castro, M. E. *Faraday Discuss.* **1999**, *114*, 313-329.

(29) Redhead, P. A. *Vacuum* **1962**, *12*, 203-211.

(30) Fukui, K.; Tero, R.; Iwasawa, Y. *Jpn. J. Appl. Phys.* **2001**, *40*, 4331-4333.

(31) Róman, E.; Bustillo, F. J.; de Segovia, J. L. *Vacuum* **1990**, *41*, 40-42.

Table 5.1 Relative yield for CH_3COOH TPD on (a) $TiO_2(001)$ and (b) $TiO_2(110)$ shown in figure 5.6a and 5.6b, respectively.

(a)

Product	Temperature (K)	Relative yield
CH_3COOH	380	trace
CH_4	430	0.12
CO_2	530	0.01
H_2	530	0.63
CO	560	0.38
CH_4	590	0.03
CH_3COOH	620	0.01
CH_2CO	630	0.02
CO	690	0.40

(b)

Product	Temperature (K)	Relative yield
CH_3COOH	410	0.02
H_2O	460	0.16
CO_2	530	0.08
CO	580	0.09
CH_2CO	580	0.36
CH_4	590	0.05
H_2O	590	0.16
H_2	600	0.16
CH_3COOH	610	0.01

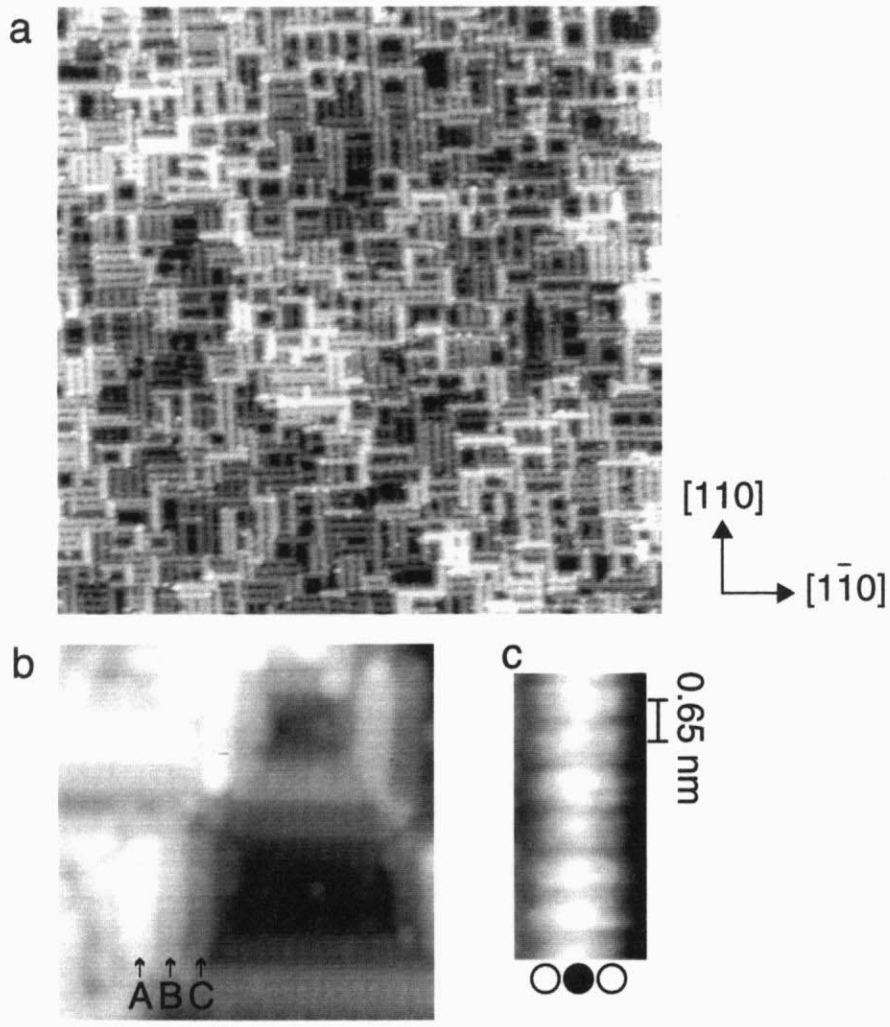

Figure 5.1

Constant current topographies (CCT) of TiO_2(001) after Ar^+-sputtering followed by annealing to 1050 K with the heating and cooling rate of 10 K s^{-1}. (a) 140x140 nm^2 (V_s: 1.70 V, I_t: 0.10 nA), (b) 15.0x15.0 nm^2 (V_s: 2.0 V, I_t: 0.04 nA), (c) 3.6x1.9 nm^2 (V_s: 2.0 V, I_t: 0.04 nA).

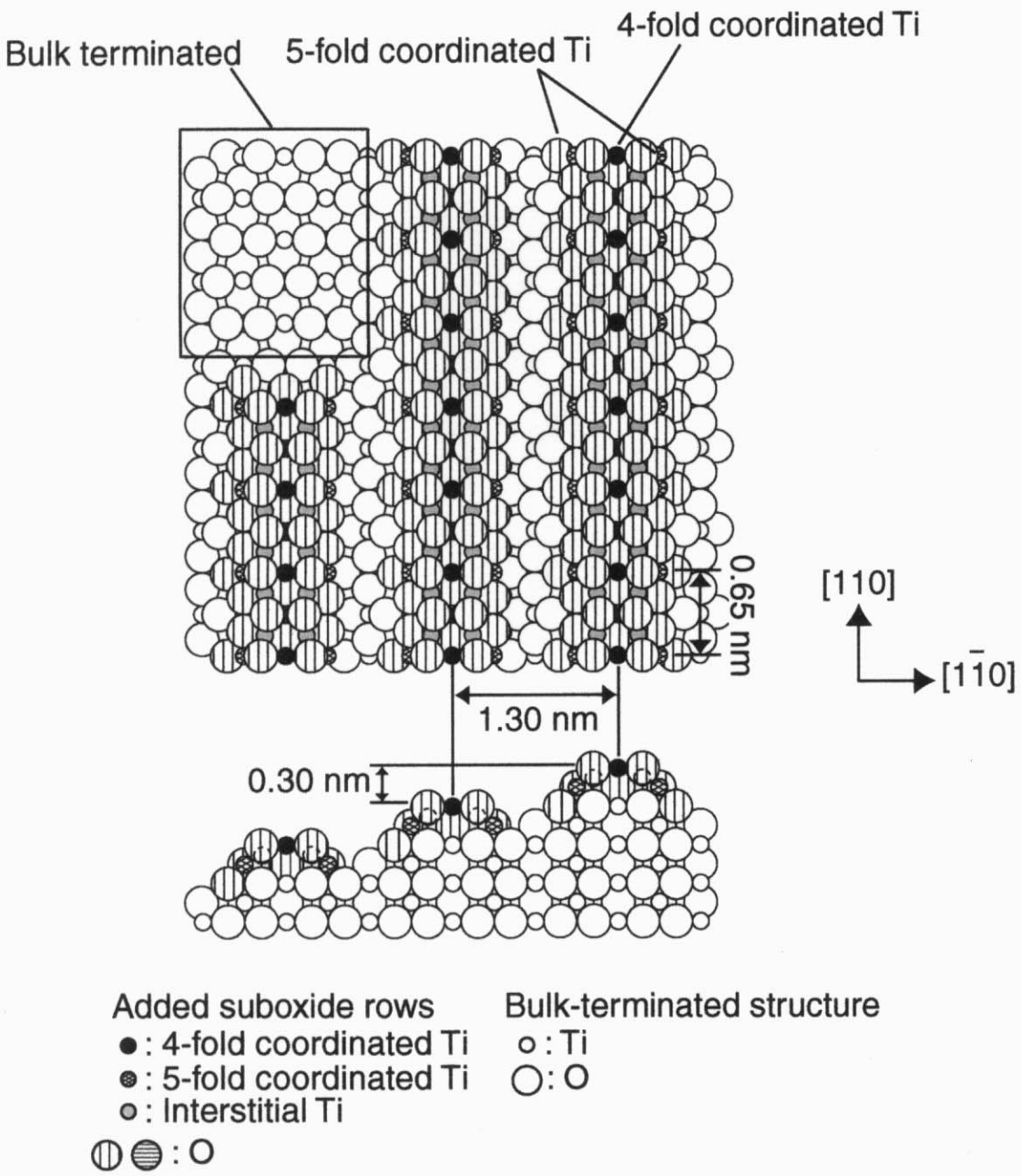

Figure 5.2

Structural model (top and side view) of the bleachers-like structure on $TiO_2(001)$.

Small and large empty circles represent Ti and O atoms in a bulk crystal, respectively. Filled, shaded and gray small circles represent fourfold coordinated, fivefold coordinated, and interstitial Ti atoms in the added suboxide rows, respectively. Shaded large circles represent O atoms of added suboxide rows.

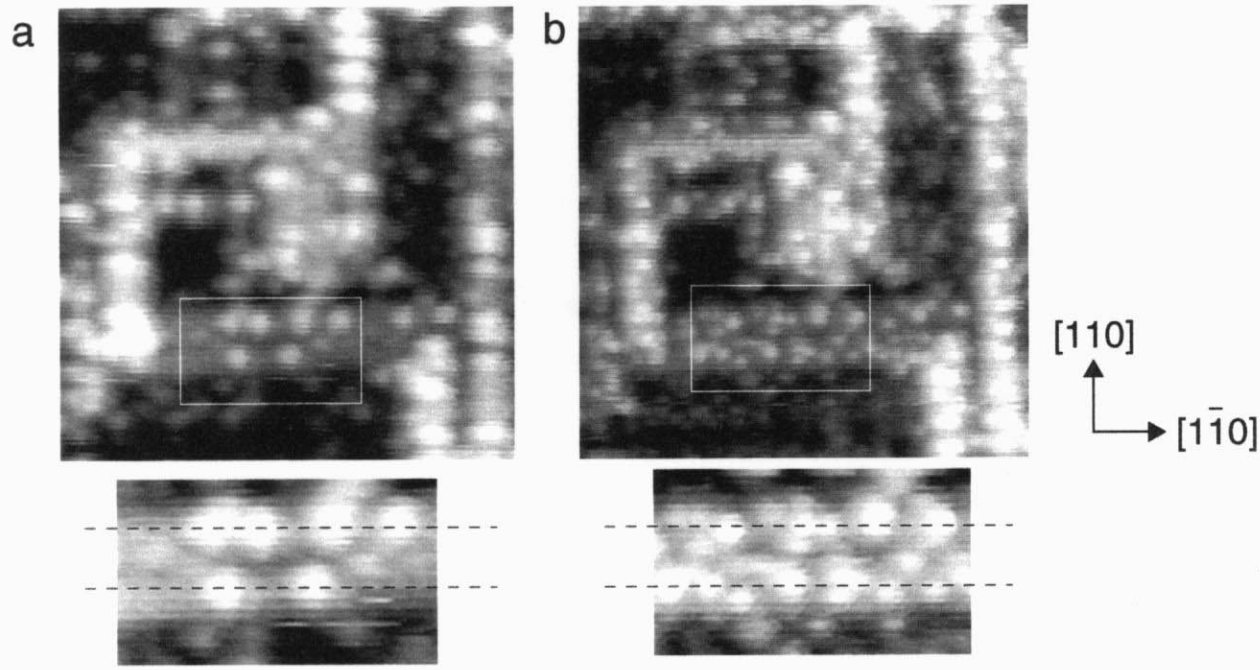

Figure 5.3

CCTs (20.0x20.0 nm^2) of TiO_2(001) after exposure to various amount of methanol and the magnified images in the white rectangulars (4.7x8.0 nm^2). Dotted lines indicate the place of fourfold coordinated Ti.
(a) 3.0 L (V_s: 1.20 V, I_t: 0.02 nA), (b) 114 L (V_s: 1.00 V, I_t: 0.05 nA).

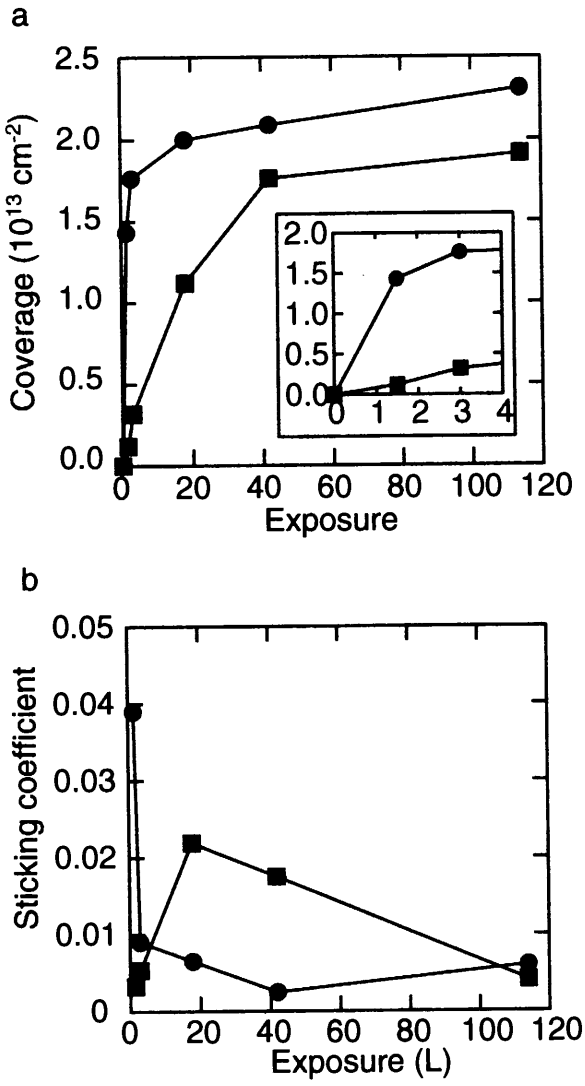

Figure 5.4

(a) Relation between methoxy coverage on fourfold coordinated Ti (filled circles) and fivefold coordinated Ti (filled squares) versus methanol exposure on TiO_2(001) at RT.

(b) Sticking coefficient of methoxy during each exposure plotted in (a).

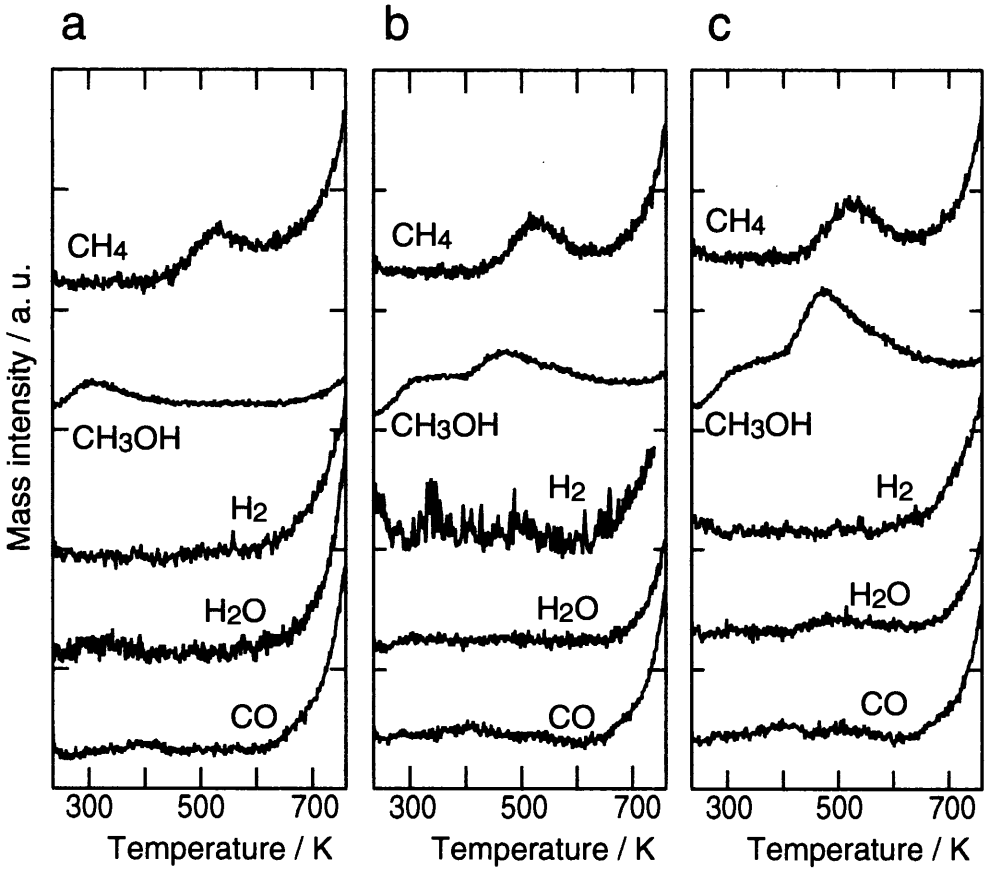

Figure 5.5

TPD spectra measured for TiO_2(001) after exposure to various amount of CH_3OH at 240 K with the heating rate of 0.6 K s^{-1}. (a) 0.1 L, (b) 1.5 L and (c) 3.0 L.

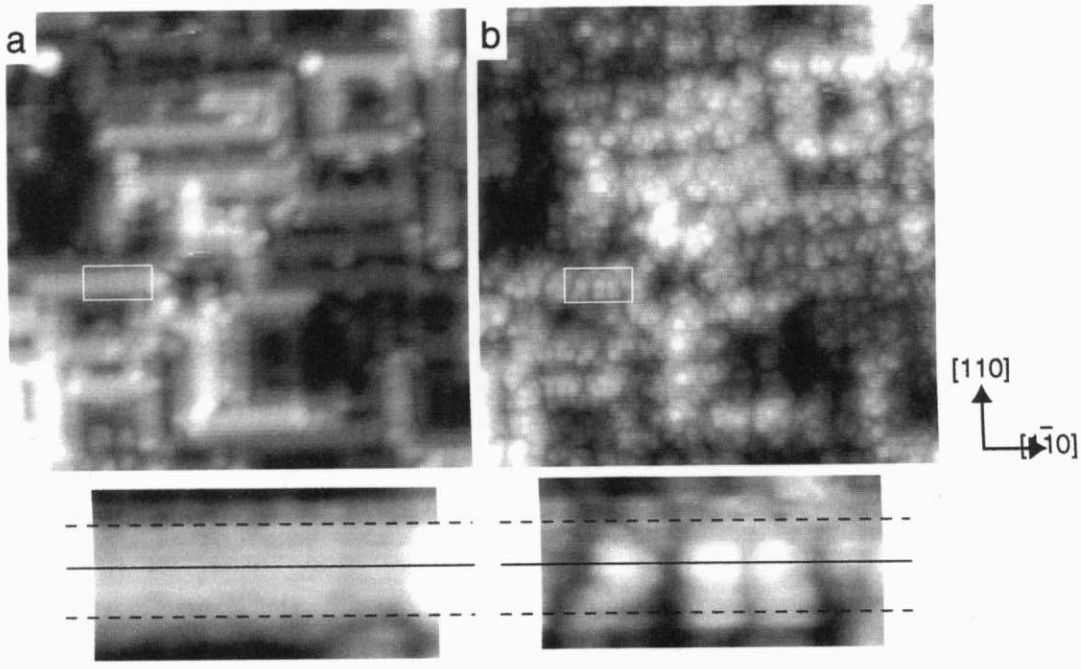

Figure 5.6

CCTs (30.0x30.0 nm^2) and the magnified images in the white rectangular (3.4x6.7 nm^2) of the same area of TiO_2(001) surface (a): before (V_s=2.00 V, I_t=0.10 nA) and (b): after (V_s=2.00 V, I_t=0.09 nA) exposure to 3.0 L of CH_3COOH.

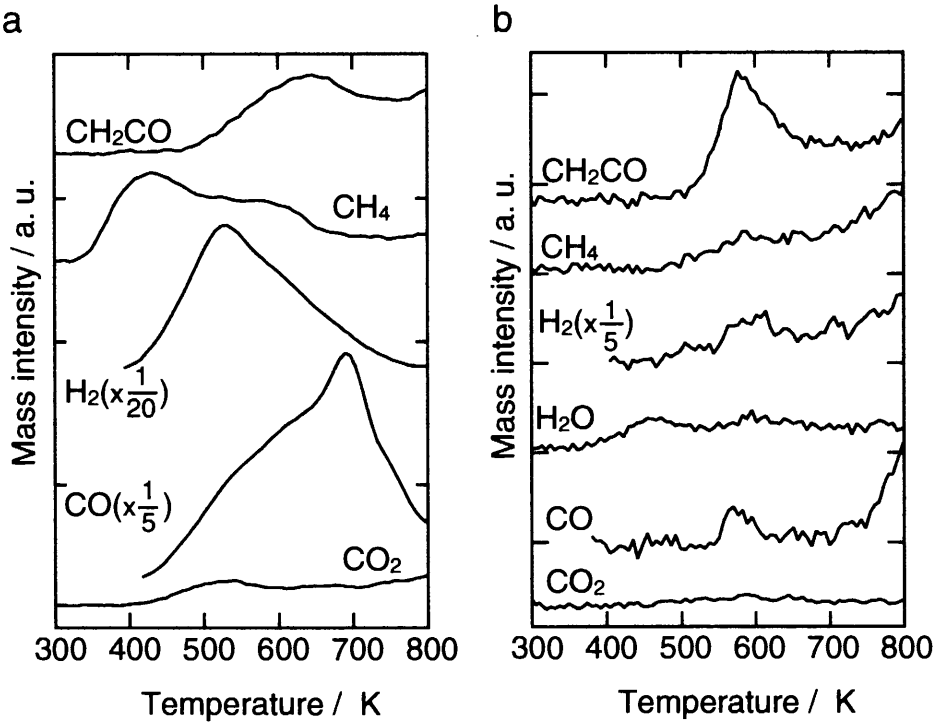

Figure 5.7

TPD spectra measured for (a): TiO_2(001) after exposure to 6.0 L of CH_3COOH at 295 K with the heating rate of 8 K s^{-1}. (b): TiO_2(110) after exposure to 4.0 L of CH_3COOH at 295 K with the heating rate of 7 K s^{-1}.

Chapter 6.

Nano-scale Assembly and Structural Transformation on TiO_2(001) Investigated by Scanning Tunneling Microscopy

Abstract

Nano-scale structures on $TiO_2(001)$ were investigated by STM. The same unit cell as the bleachers-like structure on $TiO_2(001)$ assembled a pyramidal structure and flat terraces by varying the annealing condition subsequent to Ar^+-sputtering. Nano-scale structural transformation of the bleachers-like structure occurred at 390-660 K, which was rather lower temperature than preparation of the bleachers-like structure. The effect of reduction degree of the sample bulk and molecular adsorption on nano-scale structural transformation was discussed.

6.1 Introduction

Controlling and manufacturing the size and shape of materials on nano-scale are regarded as the key issues in next generation - nanotechnology. Metal oxide particles with diameter less than 100 nm show specific character different from bulk and are applied to various industrial field such as electronic device, magnetic device, optical material, catalyst and sensor.[1] TiO_2 has especially wide use as photo- and non-photoinduced catalyst, [2,3] medial material,[4,5] pigment and so on. The surfaces of rutile-type TiO_2 are most extensively studied as a typical transition metal oxide surfaces.[6-8] TiO_2(110) surface is the most stable among the low-index planes of rutile-type and anatase-type TiO_2. [9-13] The surface structure of TiO_2(110)-(1x1) is almost identical to bulk termination as proved experimentally[14,15] and theoretically. [9,10] However, in spite of high stability, it has been reported that structure of TiO_2(110)-(1x1) surface drastically changes into several kinds of TiO_x adlayer depending on conditions. Reversible structural transformation between TiO_2(110)-(1x1) and -(1x2) over temperature range of 723 K-923 K under UHV was first reported by Møller and Wu, by means of low energy electron diffraction (LEED).[16] Recent STM studies have been revealed that TiO_2(110)-(1x2) surface consisted of "double strand" rows running along the [001] direction.[17-20] Each row was sometimes connected by "cross-linked" or "single-liked" structure. Totally considered from previous studies, (1x2) is formed at two temperature range, at 700-800 K and above 1200 K.[16,20,21] TiO_2(110)-(1x2) formed at the former can transform to (1x1),[16,21] but at the later can not.[20] Under oxygen ambient, the surface structure of TiO_2(110) changed more drastically, depending on conditions.[Onishi, 1996 #17; Li, 1998 #16; Bennett, 1999 #18]

On the other hand, there has been rather small number of studies about TiO_2(001) surface. Theoretical calculations revealed that TiO_2(001) had the most highest energy

among bulk-terminated structures of TiO_2 low-index planes.[9-11] Two kinds of ordered phases were observed by LEED depending on annealing temperature, which were assigned to two kinds of faceted structure.[22] STM and AFM studies have shown that these two phases are actually faceted or disordered structure a few tens to hundreds nm in width. Structural analysis of $TiO_2(001)$ has long been given up. Recent report on a non-equilibrium network-like $\left(7\sqrt{2}\times\sqrt{2}\right)$ phase on $TiO_2(001)$ is the only work achieving atomic-scale STM images.[23] The network-like structure was prepared by annealing above 1473 K with a heating and cooling rate of 100 K s^{-1}. The temperature was so high that partly "the crystal deformed in this temperature range".

In chapter 3 and 4, I have described and discussed about a "bleachers-like structure" on $TiO_2(001)$, which I succeed in constructing and visualizing by STM for the first time. The bleachers-like structure is corresponding with previously reported higher temperature phase judging from LEED pattern. The bleachers-like structure consisted of unit cells of 1.30x0.65 nm^2. I proposed a new structural model based on atom-resolved STM images. The model was composed of suboxide rows with stoichiometry of $Ti7O_{11}$-Ti_7O_{12} ($TiO_{1.57}$-$TiO_{1.71}$) added on each narrow terrace of bulk-terminated (114) surface. In this chapter, nano-scale structure on $TiO_2(001)$ is presented. Nano-scale assembles consisted of the same unit cells as the "bleachers-like structure" is described in the first part, and nano-scale transformation of bleachers-like structure in the second part.

6.2. Experimental

The experiments were performed in two different UHV chambers. STM images were obtained in an ultrahigh vacuum (UHV) STM (JEOL JSTM 4500VT) equipped with

an Ar^+ ion gun and a LEED optics. The base pressure was $1x10^{-8}$ Pa. A polished $TiO_2(001)$ wafer of $6.5\times1\times0.25$ mm^3 (Earth Chemical) was used after deposition of Ni film on the rear side of the sample to resistively heat the sample on a sample holder. Heating rate and cooling rate was controlled to be 7-10 K s^{-1}. The $TiO_2(001)$ surface was cleaned with cycles of Ar^+ ion sputtering (3 keV for 2 min) and annealing under UHV at ca. 900 K. All STM images displayed in this report were obtained at room temperature (RT) with electro-chemically etched W tips. The surface temperature of the crystal was monitored by an infrared radiation thermometer.

TPD spectra were measured in an UHV chamber equipped with Ar^+ ion gun, a LEED optics and quadrapole mass spectrometer. The base pressure was $1x10^{-8}$ Pa. A polished $TiO_2(001)$ wafer of $16\times8\times1$ mm^3 (Earth Chemical) with deposited Ni film on the rare side was fixed by Ta sample holder with another $TiO_2(001)$ wafer without Ni film, sandwiching a small Ta foil with a spot-welded chromel-alumel thermocouple. Exposed area of the sample available for TPD was 8×8 mm^2. TPD of $TiO_2(001)$ was performed in the same way.

Formic acid (Wako, 96 % purity) and acetic acid (Wako, 95 % purity) used in this study was purified by repeated freeze-pump-thaw cycles. Gases were introduced into the chamber by back-filling.

6.3 Results and Discussions

6.3.1 Nano-Scale Assembles on $TiO_2(001)$

In this section nano-scale assembles on $TiO_2(001)$ consisted of the same unit cell as

the bleachers-like structure depending on annealing temperature subsequent to Ar^+-sputtering. Figure 1 shows a STM image of $TiO_2(001)$ surface after annealing at 1050 K for 30 s with a heating and cooling rate of 7 K s^{-1}. The cleaning condition was nearly corresponding to that described in previous chapters. The surface was covered with flat bleachers-like structure similar to Figure 4.2 and 5.1.

Figure 2 shows a STM image of $TiO_2(001)$ surface after annealing at 1050 K for 300 s with a heating and cooling rate of 7 K s^{-1}. A pyramidal structure consisted of four equivalent {114} surfaces was observed. The atom-resolved image clearly showed that the unit cell of the pyramidal structure is the size of 1.3x0.65 nm^2 the same as that of the bleachers-like structure. It must be noted that just before the cleaning cycle, the sample has been annealed at 1200 K for 300 s, which leads to disordered phase identical to Figure 3.1d. Thus the sample surface is rather reduced comparing with Figure 6.1. Valleys, which are depletion consisted of four equivalent {114} surfaces and small domains of bleachers-like structure were also observed at other regions.

Figure 3 shows a STM image of $TiO_2(001)$ surface after annealing to 1200 K with heating rate of 20 K s^{-1}. Annealing time was 60 s. Flat terraces consisted of rows running along the [110] (terrace A) and [$1\bar{1}0$] (terrace B) directions. The difference in height between terrace A and B was ~0.15 nm, which corresponding to half height step of the bulk-terminated $TiO_2(001)$ structure. Each row seemed identical to the topmost terrace of a row in the bleachers-like structure, though high resolution imaging was difficult due to particle-like structures scattered on the surface. The annealing temperature of figure 6.3, 1200 K was corresponding to that the surface was covered by disordered particle structures (Figure 3.1d). Actually similar structure to Figure 3.1d was observed in some part of the surface. Therefore, Figure 6.3 can be regarded as halfway from terrace structure to particle-covered surface.

The results in figure 6.2 and 6.3 indicate that the bleacher-like structure is formed by competition of two processes. Rather wide (114) slope in Figure 2 resulted from long annealing time reveals "faceting" to (114) plane is thermally stable. Long [110] and $[1\bar{1}0]$ rows in figure 6.3 appeared after annealing with high heating and cooling rate. The result shows "linear growth" of suboxide rows along the [110] and $[1\bar{1}0]$ directions is favored kinetically.

One explanation for the difference in stability between "faceting" and "linear growth" is composition of each surface. The added suboxide row on the structural model of the bleachers-like structure has stoichiometry of Ti_7O_{12} on the topmost terrace and Ti_7O_{11} on other narrow terraces in the (114) slope. Figure 6.4 shows structural models of a (114) slope and a (001) terrace. On the (114) plane Ti_7O_{11} is dominant (Figure 6.4b) possibly due to oxygen desorption during long UHV annealing. On the other hand, Ti_7O_{12} is predominant on the (001) terrace (Figure 6.4b). It is also possible that entire surface energy of (001) is larger than (114), while locally more symmetrical Ti_7O_{12} is favored to Ti_7O_{11}. Further reduction of surface stoichiometry than Ti_7O_{11} ($TiO_{1.57}$), for example Ti_2O_3, may lead to disordered phase as shown in Figure 3.1d. Actually, the temperature range of formation of the bleachers-like structure became small on highly reduced surface after daily experiments for months, and finally no ordered phase could be constructed.

The terrace structure in figure 6.3 looks similar to the network-like structure in ref. [23] at a glance. However, on the network-like structure, height difference between adjacent terraces of different ridge orientation is reported to correspond to single step height, 0.3 nm. This means the periodicity along *z* axis is doubled from bulk crystal on the network-like structure, while the symmetry remains in the terrace structure in this study. Formation process of the network-like structure and the terrace structure must be completely different.

6.3.2 Nano-Scale Structural Transformation on TiO_2(001)

In this section nano-scale structural transformation from the bleachers-like structure to nano-particles at low temperature is presented. Figure 6.5 shows the STM images of the bleachers-like structure reannealed to 390-660 K from RT. The sample was kept at each temperature for 30 s. It should be noted that the sample has been reduced by daily cleaning cycles for three months and color of the sample turns to deep blue. The surface was almost completely covered with particle-like structures with diameter of 0.9-6 nm (convolution from tip shape was not considered here). The structural transformation was irreversible and the bleachers-like structure did not recovered even after annealing to 1050 K. Strange to say, slightly diffused but clearly recognizable LEED pattern was observed even after the surface was covered by particles as shown in figure 8c. We could not attain atomic resolution on the surface of the particles by STM.

It is interesting such a drastic structural change occurs at rather low temperature; the bleachers-like structure has prepared by annealing under UHV at 1050 K and once passed through the temperature range of 390-660 K during cooling. In section 6.3.1, I mentioned the possibility of the structural transformation to disordered phase by reduction, but the temperature here was too low for oxygen desorption. Henderson has reported that slower diffusion of Ti and oxygen between surface and bulk occurs at 400-700 K on Ar^+-sputtered TiO_2(110). [24] Re-oxidation of Ar^+-sputtered TiO_2(001) has also reported to occur above 560 K. [25,26] The temperature range of nano-particle growth in this study well corresponds to these studies, therefore self-diffusion of Ti and O is considered to cause the structural transformation on the bleachers-like structures. Especially diffusion of interstitial Ti^{n+}, which is in the void octahedral site of the rutile and produced by oxygen

desorption, is regarded as important factor for structural change on TiO_2(110) surface under UHV[21] and oxygen ambient.[Onishi, 1996 #17; Li, 1998 #16; Bennett, 1999 #18]

Figure 6.6 shows the bleachers-like structure on near-stoichiometric TiO_2(001) reannealed to 400-700 K. Another new sample, which experienced only a few cycles of Ar^+-sputtering and annealing, was used. The bleachers-like structure prepared by annealing to 950 K (Figure 6.6a) remained even after reannealing at 400 K (Figure 6.6b) or 700 K (Figure 6.6c) for 300 s. However, particle structures sparsely appeared when the sample was reannealed again at 590 K for 300 s subsequent to reannealing at 400 K for 300 s. These results are indicative of two points. First, the driving force of nano-particle growth is diffusion of interstitial Ti as expected. Second, there is a temperature window depending on reduction degree of the sample to form "seeds" of nano-particles. The first point is obvious comparing Figure 6.6d with Figure 6.5d. The second point is derived from Figure 6.6b and d. In order to confirm the second point, the sample was kept at 580 K for 300 s during cooling after identical cleaning procedure to Figure 6. In this case nano-particles did not appear. Thus pre-annealing at 400 K was important for nano-particle growth in Figure 6.6d. Once the "seeds" were formed, they would grow larger at higher temperature. The temperature of seeds formation would be about 400-500 K, because nano-particles smaller than Figure 6.6d appeared on the surface when the sample was kept at 490 K similarly,. The temperature range was quickly passed through in Figure 6.6c.

In order to investigate the chemical property of the particle structure, TPD of acetic acid was measured. Figure 6.7a shows TPD spectra measured for TiO_2(001) after Ar^+-sputtering and annealing to 1050 K followed by re-annealing at 500 K for 15 min. The condition corresponded to preparation for the particle-covered surface as figure 6.5d. Surface reactivity drastically changed comparing with that of the bleacher-like structure

(Figure 6.7b). Main reaction path of acetate on the particle-covered $TiO_2(001)$ turned into decomposition and decarboxylation, which was indicated from sharp desorption peaks of H_2, CO and CO_2 at 430 K. Small desorption peaks of CH_4 at 430 K and CH_2CO at 630 K similar to the bleachers-like structure would desorbed from unchanged domain due to a gradient of temperature in the sample. In previous TPD studies of acetate on TiO_2 powder and single crystal, recombinative desorption of acetic acid from acetate and hydroxyl occurred at 390-400 K and other reaction products desorbed above 500 K. Highly active Ti cations must have been exposed on the surface of the particles. It was impossible to clarify the active site because atomic scale structure of the particle surface was not resolved by STM, but highly defective surface was proposed from high reactivity. Spectroscopic methods could not be measured from apparatus reasons. For characterization of the particle structures, STS measurement may be favored to macroscopic method because properties of a structure with in this range likely vary with size due to quantum effect.[1,2]

6.3.3 Adsorbate-Induced Nano-Scale Structural Transformation

In this section, the effect of adsorbed molecules on structural change is described. Figure 6.8a shows a STM image of $TiO_2(001)$ surface after the bleachers-like structure was reannealed at 720 K for 30 s. The surface was covered by particle structures comparable to Figure 6.5. The diameter of the particle distributed around 2 nm. The distribution was similar to that of Figure 6.5d. Figure 6.8b shows a STM image of $TiO_2(001)$ after the bleachers-like structure was annealed to 710 K subsequent to exposure to 12 L of formic acid at RT. Particle structures appeared all over the surface as well, however, the size of the particles was significantly larger. The diameter distributed around 5 nm. These

experiments were performed using the same sample as Figure 6.5 within a short period, which means the degree of reduction was similar to each other. The reaction of adsorbed formate promoted the growth of the particle structure.

The most likely explanation is that oxygen atoms originally contained in formate dropped on the surface during reaction, and caught Ti cations diffused from bulk. Fixation of Ti by gas phase oxygen is the general explanation of TiO_x adlayer growth on TiO_2(110).[Onishi, 1996 #17; Li, 1998 #16; Bennett, 1999 #18] It has been reported that when a formate-adsorbed cross-linked TiO_2(110)-(1x2) structure is annealed to 570 K, (1x1) domains grows accompanying with thermal reaction of formate.[27]

Figure 6.9a and b shows STM images of the same area of the bleachers-like structure on TiO_2(001) before and after exposure to 102 L of oxygen. The sample was a rather new and near-stoichiometric. No feature derived from oxygen was observed in figure 6.9b. However, when the surface was annealing to 420 K, the surface was completely covered up with particle structures (Figure 6.9c and d). As explained at last paragraph, it is probable that adsorbed oxygen caught the diffused interstitial Ti and fixed on the surface as TiO_x particles. Figure 6.9e shows the reannealed surface on the same sample as Figure 6.9a-d at 400 K without oxygen exposure. No structural change took place. Therefore, it was concluded that oxygen adsorbed on the bleachers-like structure at RT though it was invisible to STM, and caused the structural transformation at 420 K.

It has been proposed that oxygen molecule dissociatively adsorbed at bridge oxygen defect and dose not on fivefold-coordinated Ti on a perfect TiO_2(110)-(1x1) domain.[28] One oxygen atom filled the defect and the other diffuse on the surface as atomic oxygen. In the case of the bleachers-like structure, it is likely that fourfold coordinated Ti is dissociative adsorption of oxygen. High reactivity of the fourfold coordinated Ti has been described in chapter 4 and 5. Possibility of oxygen defect sites as

dissociative adsorption can not be denied but is rather bare considered form high density of oxygen-induced particles. Invisibility of oxygen to STM is likely due to fast diffusion of atomic oxygen on the surface.

6.4 Summary

Nano-scale structures on $TiO_2(001)$ surface was investigated by STM. Controlling the annealing conditions, the unit cell of the bleachers-like structure assembled to different structures in nano-scale, such as pyramidal structure and flat terraces. On a highly reduced sample, a bleachers-like structure transformed into nano-scale particle structures by annealing at rather lower temperature than that to prepare the bleachers-like structure. Formation of "seeds" was important to growth of particles. Temperature range of seeds formation was limited and depended on the reduction degree of the sample bulk. Pre-adsorption of formic acid and oxygen promoted the growth of nano-particle structure. The mechanism would be explained by that fixation of diffused interstitial Ti cations by adsorbed atomic oxygen.

References

(1) Ichinose, N.; Ozaki, Y.; Kasyu, S. *Superfine Particle Technology*; Springer-Verlag: London, 1992.

(2) Linsebigler, A.; Lu, G.; Yates Jr., J. T. *Chem. Rev.* **1995**, *95*, 735-758.

(3) Iwasawa, Y. *Stud. Surf. Sci. Catal.* **1996**, *101*, 21-34.

(4) Kilpadi, D. V.; Weimer, J. J.; Lemons, J. E. *Coll. Surf. A: Physicochem. Eng. Aspects* **1998**, *135*, 89-101.

(5) Kilpadi, D. V.; Raikar, G. N.; Liu, J.; Lemons, J. E.; Vohra, Y.; Gregory, J. C. *J. Biomed. Mater. Res.* **1998**, *40*, 646-659.

(6) Henrich, V. E.; Cox, P. A. *The Surface Science of Metal Oxides*; Cambridge University Press: Cambridge, 1996.

(7) Lai, X.; Clair, T. P. S.; Valden, M.; Goodman, D. W. *Prog. Surf. Sci.* **1998**, *59*, 25-52.

(8) Diebold, U. The Structure of TiO_2 Surfaces. In *Oxide Surfaces - The Chemical Physics of Solid Surfaces*; Woodruff, D. P., Ed.; Elsevier: Amsterdam, 2001; Vol. 9; pp 443-484.

(9) Ramamoorthy, M.; Vanderbilt, D.; King-Smith, R. D. *Phys. Rev. B* **1994**, *49*, 16721-16727.

(10) Muscat, J.; Harrison, N. M.; Thornton, G. *Phys. Rev. B* **1999**, *59*, 15457-15463.

(11) Cox, P. A.; Dean, F. W. H.; Williams, A. A. *Vacuum* **1983**, *33*, 839-841.

(12) Lazzeri, M.; Vittadini, A.; Selloni, A. *Phys. Rev. B* **2001**, *63*, 155409-155401-155409.

(13) Lazzeri, M.; Vittadini, A.; Selloni, A. *Phys. Rev. B* **2002**, *65*, 119901(E).

(14) Maschhoff, B. L.; Pan, J. M.; Madey, T. E. *Surf. Sci.* **1991**, *259*, 190.

(15) Charlton, G.; Howes, P. B.; Nicklin, C. L.; Steadman, P.; Taylor, J. S. G.; Muryn, C. A.; Harte, S. P.; Mercer, J.; McGrath, R.; Norman, D.; Turner, T. S.; Thornton, G. *Phys. Rev. Lett.* **1997**, *78*, 495-498.

(16) Møller, P. J.; Wu, M.-C. *Surf. Sci.* **1989**, *224*, 265-276.

(17) Onishi, H.; Iwasawa, Y. *Surf. Sci.* **1994**, *313*, L783-L789.

(18) Novak, D.; Garfunkel, E.; Gustafsson, T. *Phys. Rev. B* **1994**, *50*, 5000-5003.

(19) Sander, M.; Engel, T. *Surf. Sci.* **1994**, *302*, L263-L268.

(20) Onishi, H.; Fukui, K.; Iwasawa, Y. *Bull. Chem. Soc. Jpn.* **1995**, *68*, 2447-2458.

(21) Xu, C.; Lai, L.; Zajac, G. W.; Goodman, D. W. *Phys. Rev. B* **1997**, *56*, 13464-13482.

(22) Firment, L. E. *Surf. Sci.* **1982**, *116*, 205-216.

(23) Nörenberg, H.; Dinelli, F.; Briggs, G. A. D. *Surf. Sci.* **1999**, *436*, L635-L640.

(24) Henderson, M. A. *Surf. Sci.* **1999**, *419*, 174-187.

(25) Idriss, H.; Barteau, M. A. *Catal. Lett.* **1994**, *26*, 123.

(26) Lusvardi, V. S.; Barteau, M. A.; Chen, J. G.; Eng, J.; Fruhberger, B.; Teplyakov, A. *Surf. Sci.* **1998**, *397*, 237-250.

(27) Bennett, R. A.; Stone, P.; Smith, R. D.; Bowker, M. *Surf. Sci.* **2000**, *454*, 390-395.

(28) Epling, W. S.; Peden, C. H. F.; Henderson, M. A.; Diebold, U. *Surf. Sci.* **1998**, *412/413*, 333-343.

Figure 6.1

A constant current topograph (CCT) (36.1x36.1 nm^2, V_s: 2.0 V, I_t: 0.10 nA) of a standard bleachers-like structure on $TiO_2(001)$ prepared by annealing to 1050 K subsequent to Ar^+-sputtering.

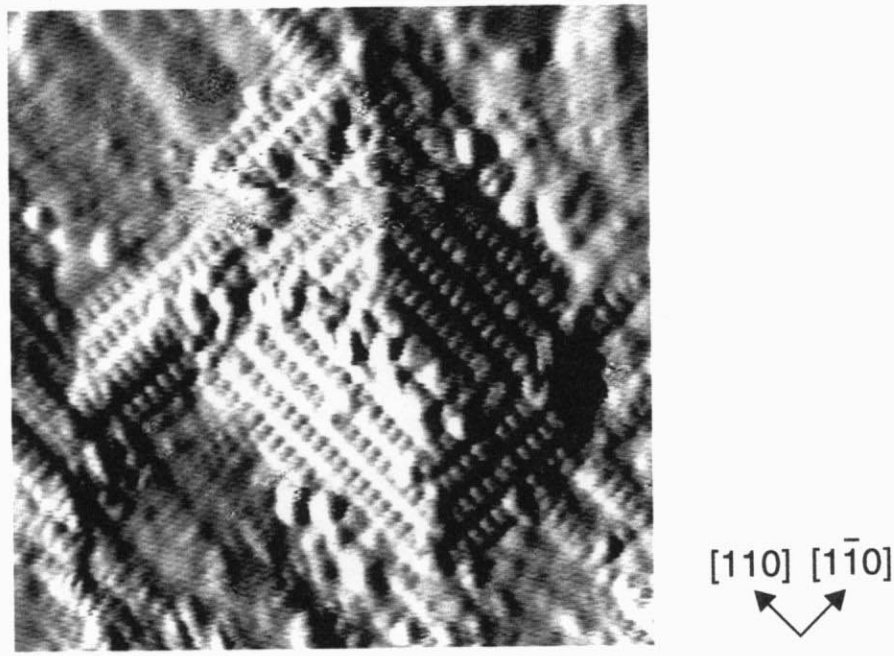

Figure 6.2

A variable current image (27x27 nm^2, V_s: +2.0 V, I_t: ~0.1 nA) of a pyramidal structure on TiO_2(001) after annealing an Ar^+-sputtered surface at 1050 K for 5 min.

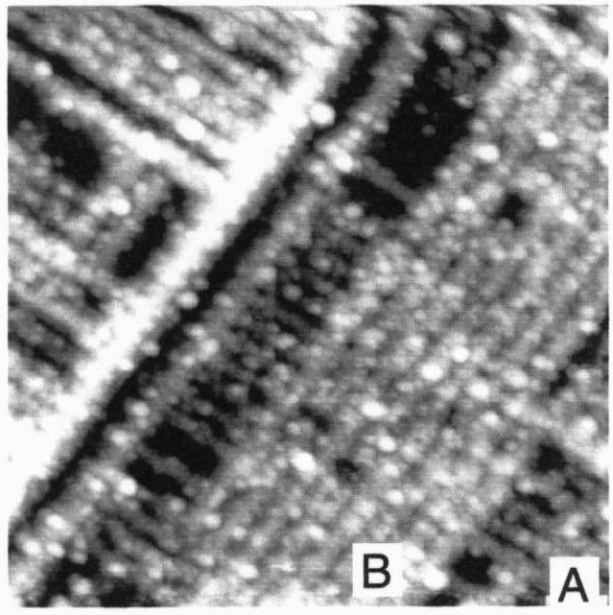

Figure 6.3

A CCT image (50.0x50.0 nm^2) of TiO_2(001) surface annealed at 1200 K with a heating and cooling rate of 20 K s^{-1}. V_s: +2.0 V, I_t: 0.12 nA.

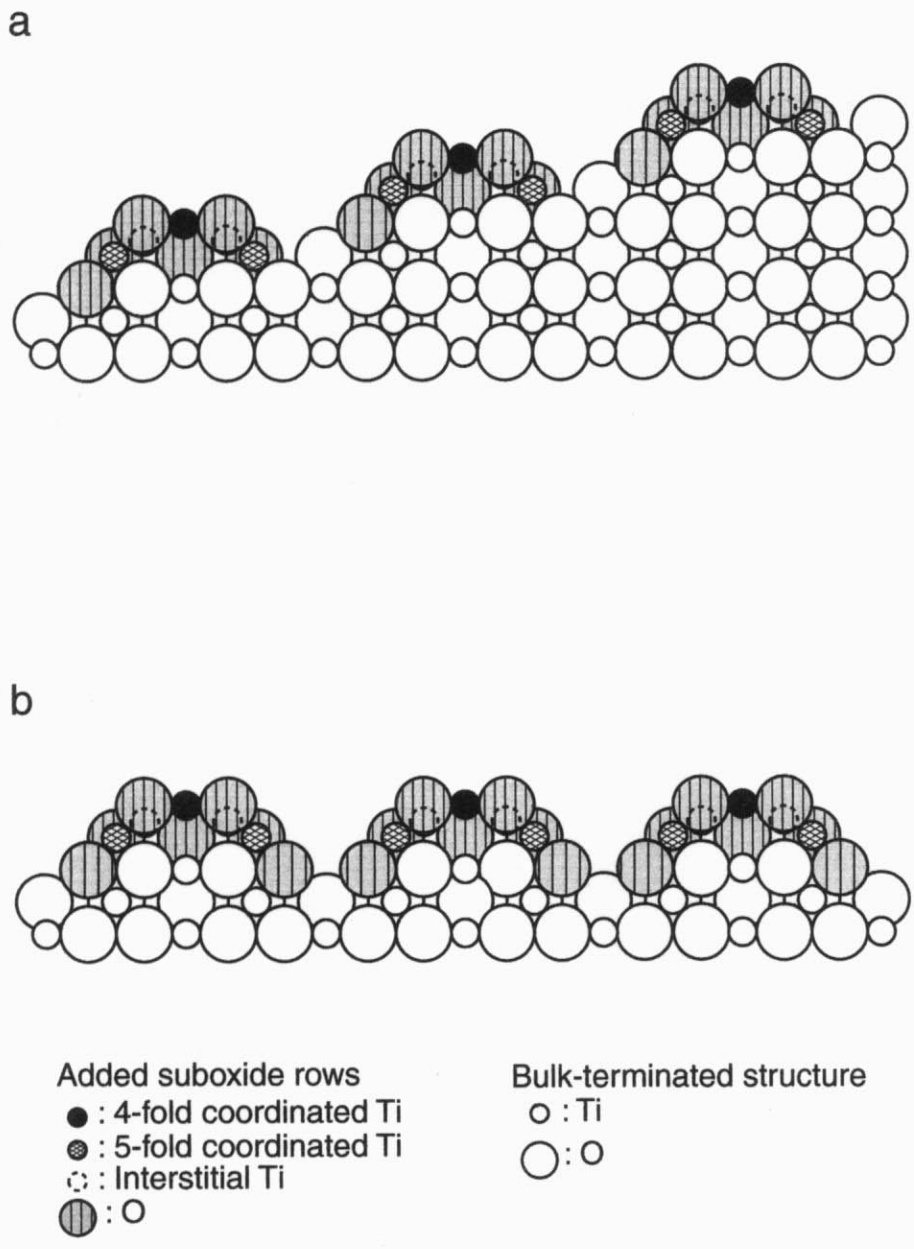

Figure 6.4

Structural models of (a) pyramidal structure shown in Figure 6.2, and (b) terrace structure in Figure 6.3 standing on the model of the bleachers-like structure. Added suboxide rows are represented shaded circles. Stoichiometry of added layer was (a) Ti_7O_{11} and (b) Ti_7O_{12}.

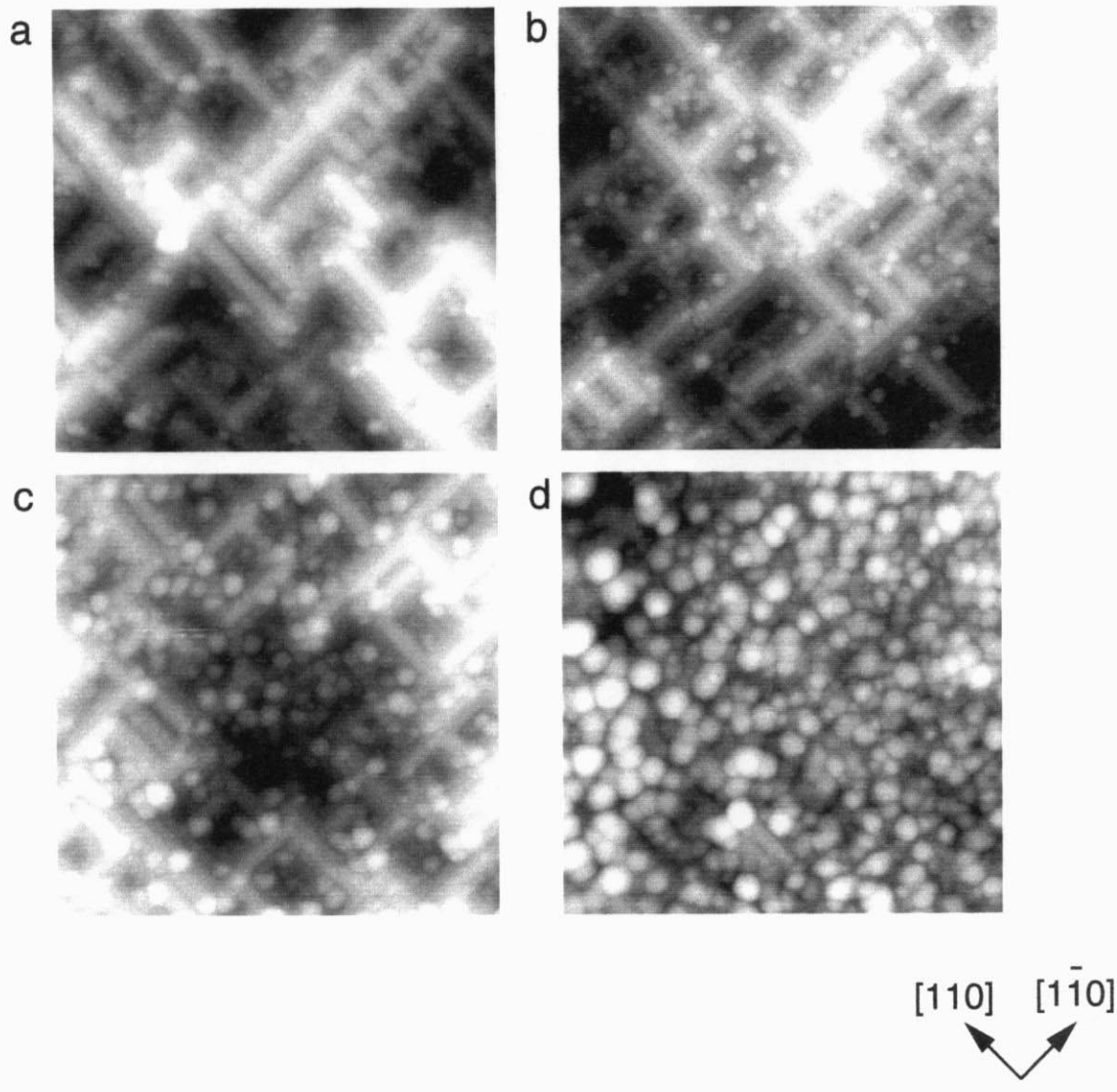

Figure 6.5

CCTs (50x50 mn^2, V_s: 2.0 V, I_t: 0.10 nA) of the bleacher-like structure on $TiO_2(001)$ reannealed from RT to various temperature. (a) 390 K, (b) 560 K, (c) 600 K and (d) 660 K.

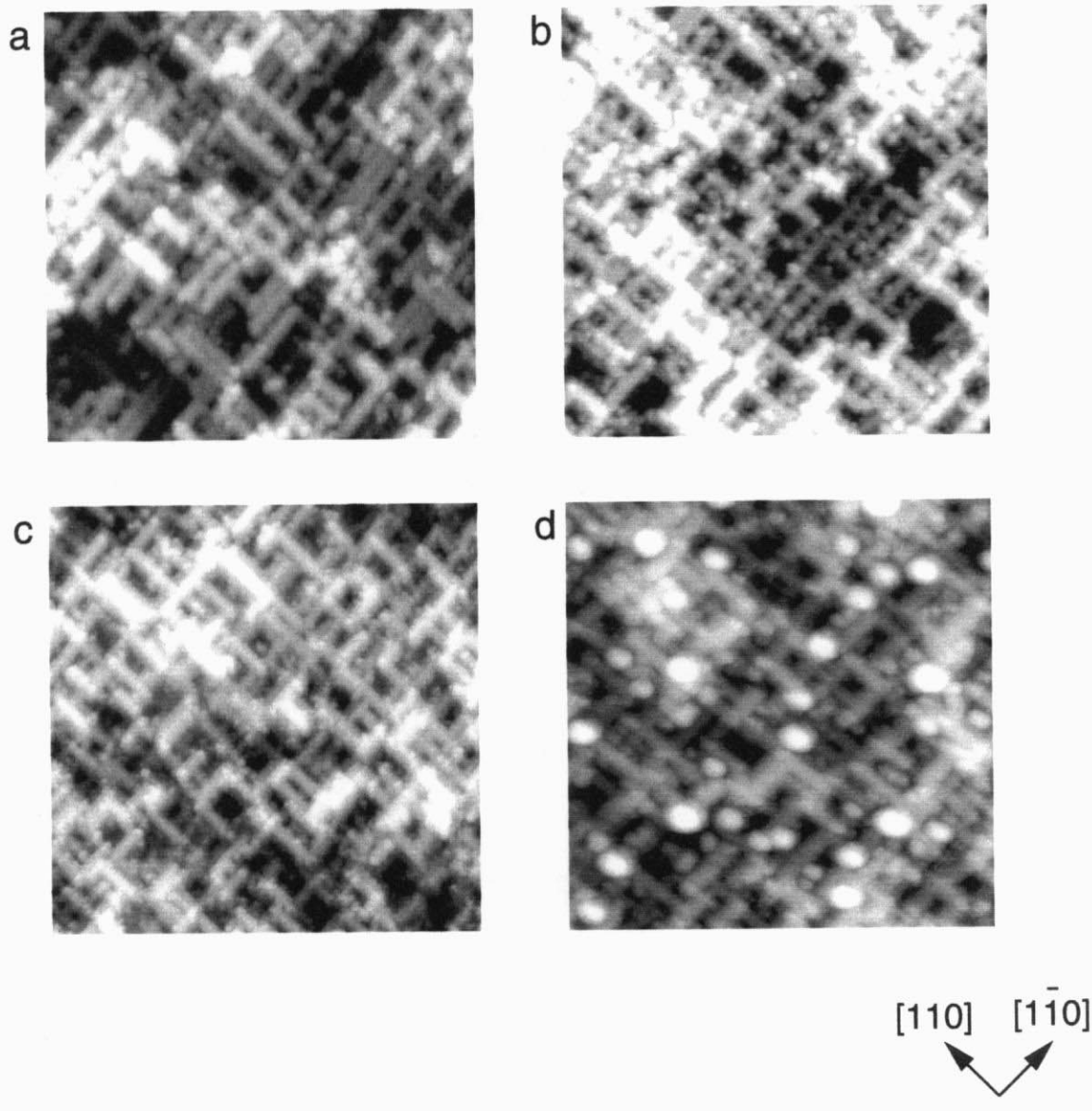

Figure 6.6

CCTs (50x50 nm^2) of the bleachers-like structure on TiO_2(001) produced by Ar^+-sputtering and annealing to 950 K was reannealed from RT to various temperature. (a) Before reannealing (V_s: 2.0 V, I_t: 0.10 nA), (b) 400 K (V_s: 2.0 V, I_t: 0.10 nA), (c) 730 K (V_s: 1.8 V, I_t: 0.10 nA). (d) (b) was annealed to 590 K (V_s: 1.8 V, I_t: 0.10 nA).

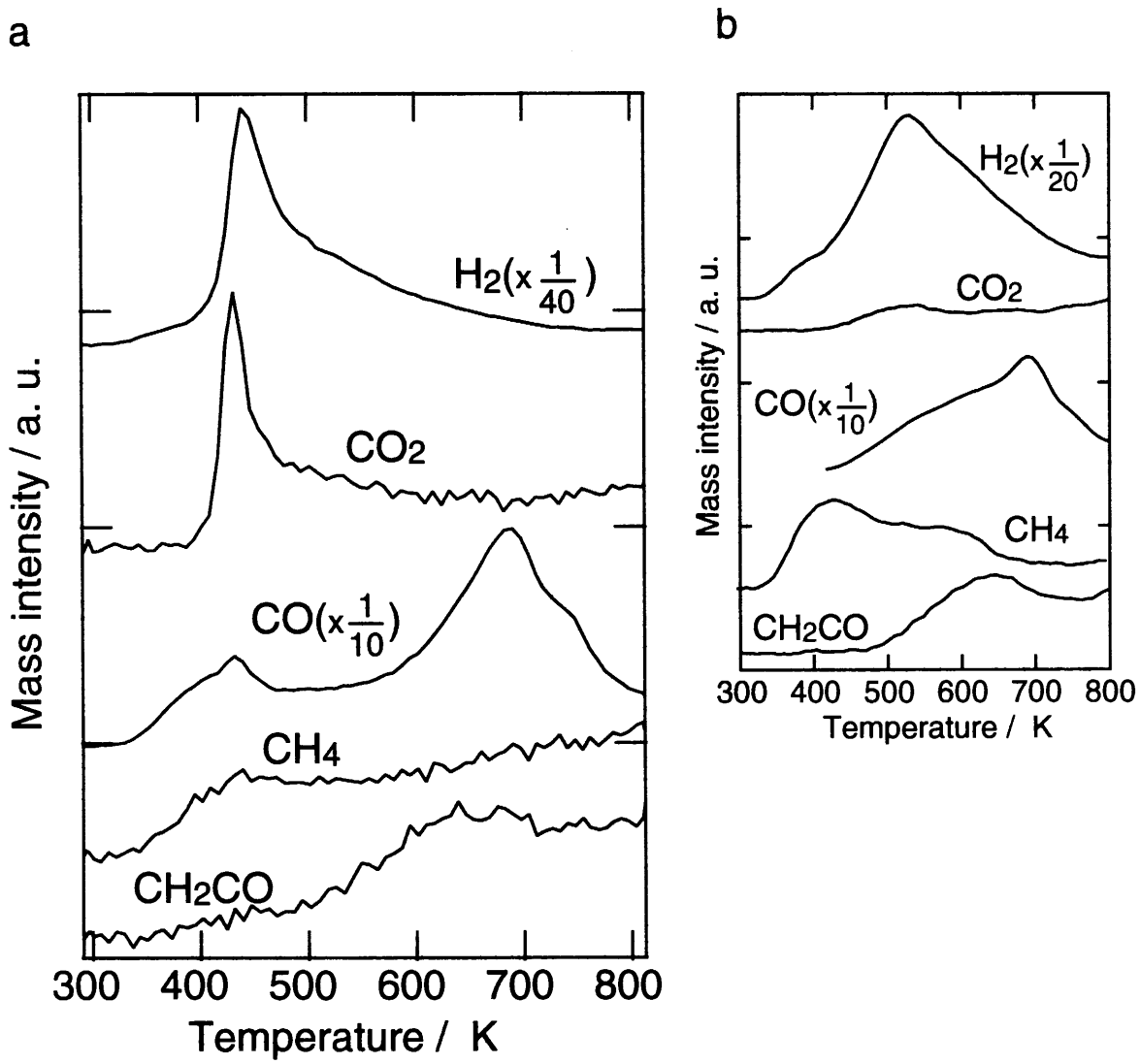

Figure 6.7

(a) TPD spectra of acetic acid on $TiO_2(001)$ reannealed at 500 K for 15 min after Ar^+-sputtering and anealing at 1050 K. The procedure corresponded to covering the bleachers-like structure with nano-particles.

(b) TPD spectra of acetic acid on the bleachers-like structure on $TiO_2(001)$.

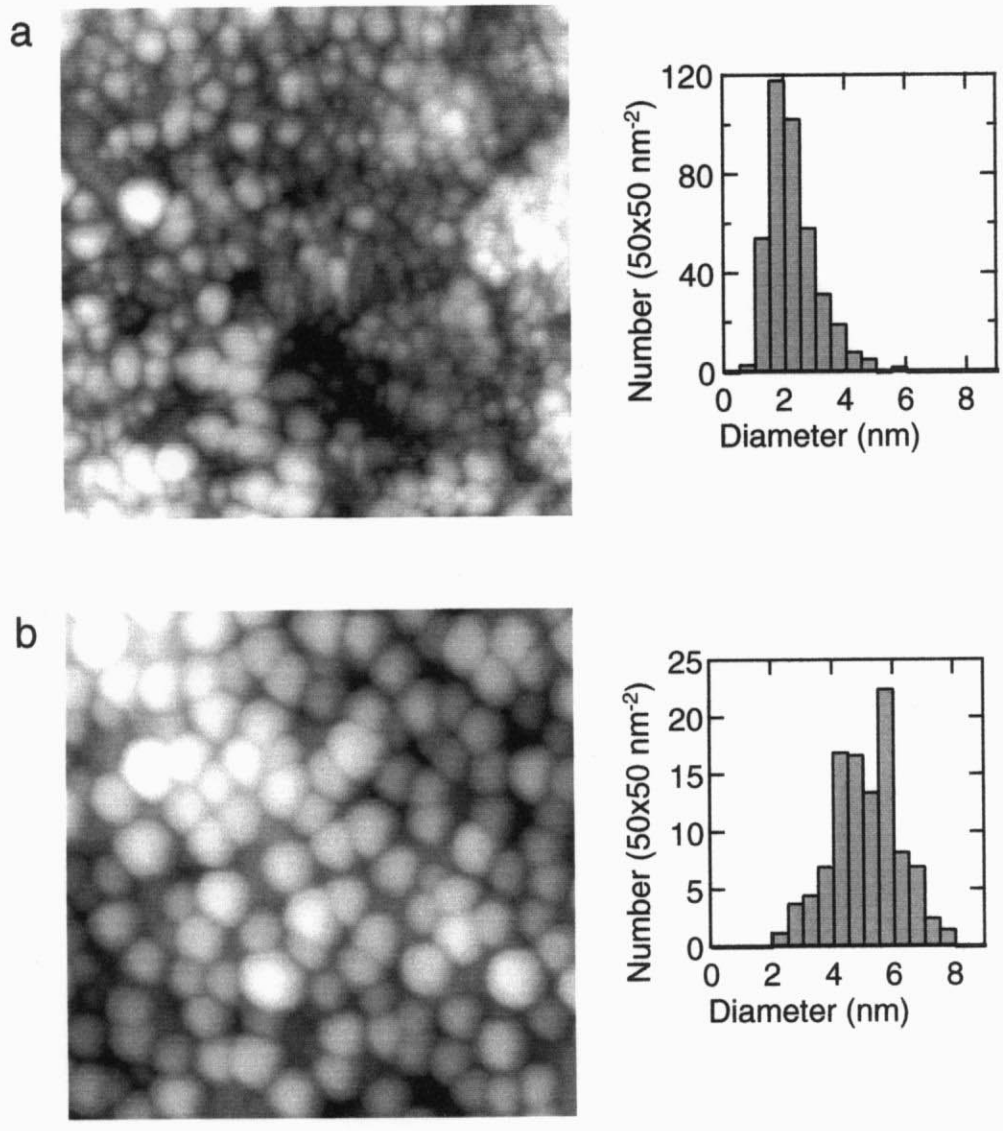

Figure 6.8

CCTs (50x50 nm^2) of TiO_2(001). (a) The belachers-like structure was reannealed to 720 K (V_s: 2.0 V, I_t: 0.10 nA). (b) The bleachers-like structure exposed to 12 L of formic acid at RT was annealed to 710 K.

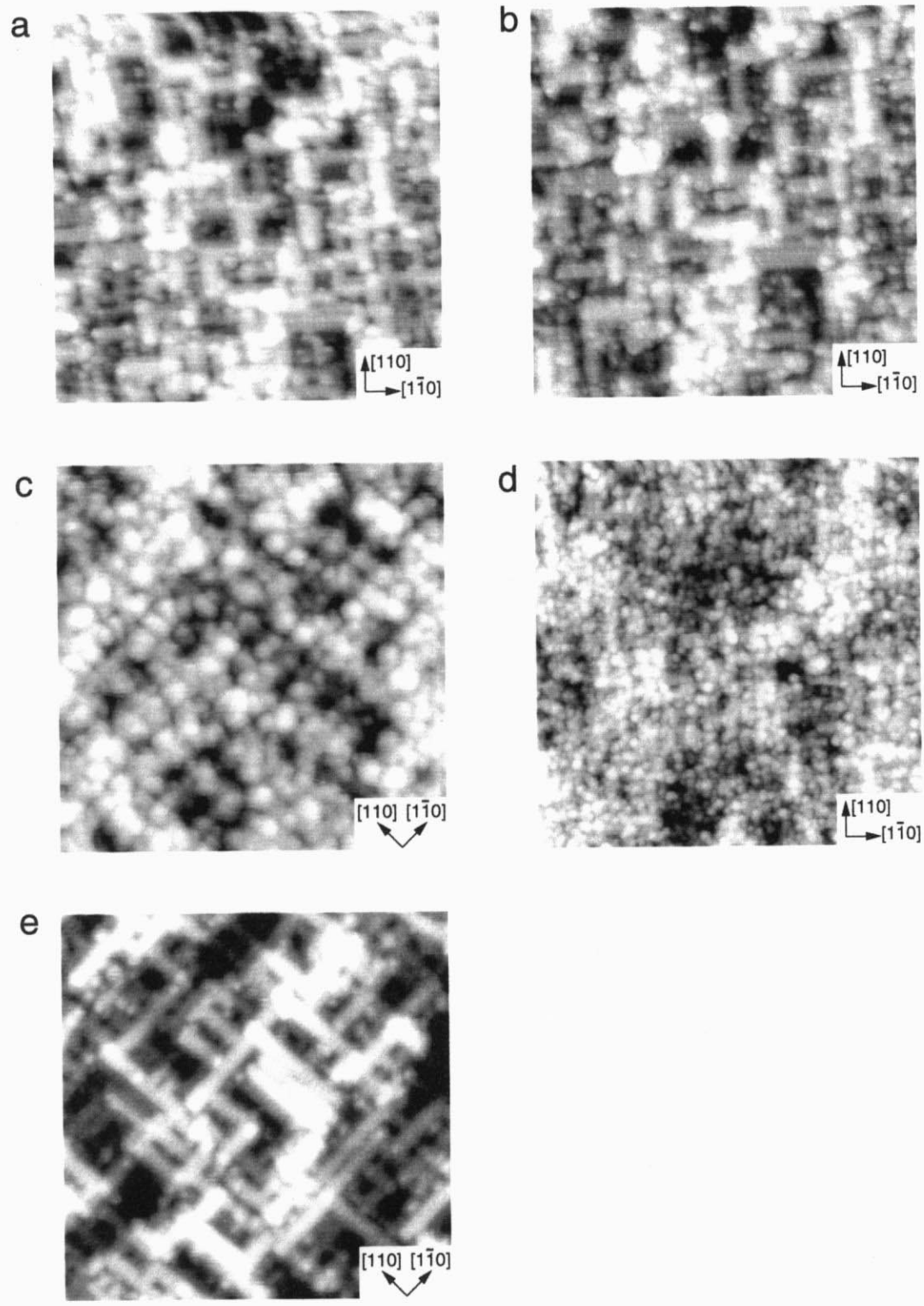

Figure 6.9

CCTs of TiO_2(001). (a) The bleachers-like structure produced by Ar^+-sputtering and annealing to 950 K (40x40 nm^2, V_s: 2.0 V, I_t: 0.10 nA). (b) The same area as (a) after exposed to 102 L of O_2 at RT (40x40 nm^2, V_s: 2.0 V, I_t: 0.10 nA). (c), (d) b was annealed at 424 K for 300 s (c: 40x40 nm^2, V_s: 2.0 V, I_t: 0.10 nA, d: 40x40 nm^2, V_s: 2.0 V, I_t: 0.10 nA). (e) The bleachers-like structure without O_2 exposure annealed at 410 K for 300 s (40x40 nm^2, V_s: 2.0 V, I_t: 0.10 nA).

Chapter 7.

Concluding Remarks

In the doctoral course, I have investigated the surface structure and chemical property of rutile $TiO_2(001)$ surface on atomic scale and on nano scale, for the purpose of development of a new reaction field and further understanding of titanium dioxide surface. Atomic scale surface structure of $TiO_2(001)$ has been an important issue in itself, and unique reactivity has been expected due to low ligand coordination of surface atoms on the bulk-terminated structure.

In chapter 3, I investigated the surface morphology of $TiO_2(001)$ depending on sample treatment by means of STM. The surface was easily turned into facet or disordered structure as reported previously. Large plateau structure and particle-like protrusions appeared on the surface after annealing the Ar^+-sputtered $TiO_2(001)$ surface to 970 K and 1160 K, respectively. I sensitively controlled cleaning conditions, such as Ar^+-sputtering intensity, annealing temperature and heating and cooling rate, and finally succeeded in constructing a flat and atomically ordered "bleachers-like" structure. The new structure consisted of crossed rows running along the [110] and $[1\bar{1}0]$ directions. Each row had a shape of "bleachers", forming narrow terraces and steps on its both slopes. It was the first achievement of constructing and visualizing well-ordered homogeneous structure on $TiO_2(001)$ surface.

In chapter 4, the new structure on $TiO_2(001)$ was examined in detail by means of LEED and STM. LEED pattern and its dependence of movement on incident beam energy indicated that the structure corresponded to one of the previously reported phases, which had been proposed as {114}-faceted structure. Atom-resolved STM images revealed that the bleachers-like structure had the identical long-range periodicity to the {114}-faceted structure, but the local structure on atomic scale was completely different. Therefore I proposed a new structural model based on atom-resolved STM images. Adsorption sites of formic acid and methanol were adopted as a probe to verify the validity of the structural

model. Both of STM images and molecular adsorptions indicated existence of two kinds of coordinatively unsaturated Ti cation. They were assigned to fivefold and fourfold coordinated Ti cations on the new structural model. It was also revealed that the bleachers-like structure was stable during thermal reactions of formic acid and methanol.

In chapter 5, I investigated the chemical property of the bleachers-like structure. Adsorption and reaction of methanol and acetic acid were studied by STM and TPD. Totally the bleachers-like structure showed high and completely different reactivity comparing with $TiO_2(110)$. Methanol adsorption and reaction evidently revealed the distinct reactivity of two Ti cations on the surface. Dissociative adsorption of methanol and decomposition of methoxy to methane occurred on Ti which was assigned to fourfold coordination in chapter 4. Methoxy on the other Ti assigned to fivefold coordination desorbed as methanol. In the thermal reaction of acetate, decomposition to CH_4 and dehydration to CH_2CO occurred at 430 K and 620 K, respectively. The active site of the former reaction was suggested to fourfold coordinated Ti and the later reaction to fivefold coordinated Ti comparing with the results that CH_2CO was dominant reaction product of acetate on $TiO_2(110)$.

In chapter 6, nano-scale structures on $TiO_2(001)$ are described. I found that the unit cell of the bleachers-like structure assembled on nano-scale to a pyramidal structure and flat terraces depending on annealing conditions. Besides, surface morphology drastically changed from atomically ordered structure to nanoparticles by reannealing at rather low temperature. The structural transformation highly depended on reduction of degree of the sample. The mechanism could be partly explained by diffusion of interstitial Ti^{n+} ($n \leq 3$) to the surface, but formation of "seed" in limited temperature range was necessary for particle growth. Pre-adsorption of formate and oxygen extremely promoted the particle growth. Atomic oxygen dropped from formate or dissociatively

adsorbed oxygen was effectively fix the diffusing Ti on the surface.

In these works, I have revealed the surface structure of TiO_2(001) on atomic scale for the first time and demonstrated the usefulness as adsorption and reaction field, and further evidently distinguished the active sites. Moreover, I believe that homogeneous arrangement of two kinds of metal cations and nano-scale self-assemblies on the "bleachers-like structure" of TiO_2(001) are quite promising from material point of view. I hope this thesis becomes meaningful step for the progress of nanotechnology in the future.

Acknowledgement

All of studies in my doctoral course were carried out under supervision of Prof. Y. Iwasawa. I would like to express here a million of gratitude to him for the opportunity to meet this attractive theme. I also appreciate thorough guidance and profitable discussions Assistant Prof. K. Fukui have given me. This thesis could not take a form without his tremendous support.

I am very much grateful to Assistant Prof. T. Sasaki and Assistant Prof. T. Shido for so much assistance. I am also grateful to Dr. S. Suzuki. He taught me operation of apparatus and procedure of tip and sample within and beyond manuals. I can not thank enough Prof. T. Urisu for his heartfelt support. I would like to thank S. Takakusagi and Y. Namai, simultaneous doctoral candidates. I really enjoyed discussion and spending in laboratory with them. Earnest thanks go to all students and associate researchers of Iwasawa laboratory for a great deal of supports and collaborations.

At last, I am truly thankful to my family, especially my parents from bottom of my heart for continuous support and encouragement.